UNIVERSITY OF MANITOBA

THE EFFECT OF PRIOR DEFORMATION ON THE AGING CHARACTERISTICS OF A CO-NI BASE SUPERALLOY

BY

G. MITCHELL OMICHINSKI

A THESIS SUBMITTED TO THE FACULTY OF GRADUATE STUDIES
IN PARTIAL FULFILLMENT OF THE REQUIREMENTS FOR
THE DEGREE OF MASTER OF SCIENCE OF MECHANICAL ENGINEERING

DEPARTMENT OF MECHANICAL ENGINEERING

WINNIPEG, MANITOBA

FEBRUARY, 1977.

"THE EFFECT OF PRIOR DEFORMATION ON THE AGING CHARACTERISTICS OF A CO-NI BASE SUPERALLOY"

by

G. MITCHELL OMICHINSKI

A dissertation submitted to the Faculty of Graduate Studies of the University of Manitoba in partial fulfillment of the requirements of the degree of

MASTER OF SCIENCE

© 1977

Permission has been granted to the LIBRARY OF THE UNIVERSITY OF MANITOBA to lend or sell copies of this dissertation, to the NATIONAL LIBRARY OF CANADA to microfilm this dissertation and to lend or sell copies of the film, and UNIVERSITY MICROFILMS to publish an abstract of this dissertation.

The author reserves other publication rights, and neither the dissertation nor extensive extracts from it may be printed or otherwise reproduced without the author's written permission.

ABSTRACT

The effects of room temperature prior deformation on the precipitation of a Co-Ni based alloy (40% Co, 38% Ni, 17% Cr, 5% Nb) were investigated. The mechanical properties and microstructures for light (5%), moderate (30%), and heavy (60%) deformations were compared with the solution treated condition. Aging was carried out at 800° C for times up to 150 hours. Cold work results in deformation twinning of the matrix. The main precipitate phase on aging is plate-shaped Ni_3Nb orthorhombic. In general, deformation accelerates this precipitation with matrix-twin interfaces acting as nucleation sites. Prior heavy deformation and aging results in partial recrystallization of the matrix. The new recrystallizing grain boundaries act as nucleation sites for discontinuous precipitation of Ni_3Nb orthorhombic in the shape of distorted spheres. The space group symmetry for both particle shapes was identified as Pma2. Improvements in tensile properties on aging the solution treated condition were more significant than those observed for deformed-aged conditions.

ACKNOWLEDGEMENTS

I would like to express my thanks to my supervisor, Dr. M. C. Chaturvedi for his support and avice. Also, I would like to thank Dr. Nabil Ibrahim and Dr. David Tseng for their helpful discussions. Finally, I am eternally grateful to my parents.

TABLE OF CONTENTS

Page

ABSTRACT i

ACKNOWLEDGEMENTS ii

TABLE OF CONTENTS iii

LIST OF FIGURES v

CHAPTER 1 INTRODUCTION 1

CHAPTER 2 LITERATURE SURVEY 3
- 2.1 Plastic Deformation 3
  - 2.1.1 Dislocations and Mechanical Properties . . . 3
  - 2.1.2 Dislocation Arrangement in the Annealed State 4
  - 2.1.3 Dislocation Arrangement in Polycrystals Deformed at Room Temperature 8
  - 2.1.4 Deformation Twinning 9
    - 2.1.4.1 General Characteristics 9
    - 2.1.4.2 Twinning Mechanism for FCC metals. . 13
- 2.2 Precipitation Hardening 15
  - 2.2.1 General Concepts 15
  - 2.2.2 Effects of Prestrain in Precipitation Characteristics 26
- 2.3 Post Deformation Annealing 29
  - 2.3.1 Recovery 30
  - 2.3.2 Recrystallization 31
  - 2.3.3 Recrystallization of Two Phase Alloys 37

CHAPTER 3 EXPERIMENTAL TECHNIQUES 53
- 3.1 Alloy Fabrication 54
- 3.2 Mechanical Properties 54
- 3.3 Precipitate Extraction 54
- 3.4 Optical Metallography 55

Page

3.5 Electron Microscopy 54
  3.5.1 Extraction Replicas 55
  3.5.2 Thin Foils 56

CHAPTER 4 EXPERIMENTAL RESULTS 57
4.1 Hardness Measurements and Tensile Testing 57
4.2 Optical Metallography 64
4.3 Precipitate Extraction and X-Ray Analysis 74
4.4 Electron Microscopy 74
  4.4.1 Precipitation Extraction 74
  4.4.2 Thin Foil Electron Microscopy 78
    4.4.2.1 As Solution Treated 78
    4.4.2.2 As Deformed 78
    4.4.2.3 Aging of the Lightly Deformed Material 85
    4.4.2.4 Aging of the Moderately Deformed Material 87
    4.4.2.5 Aging of the Heavily Deformed Material 91

CHAPTER 5 DISCUSSION 103

CHAPTER 6 CONCLUSIONS 122

APPENDIX A 123

APPENDIX B 144

REFERENCES 147

LIST OF FIGURES

NO PAGE

1 Stored energy and fraction of total deformation energy stored with elongation of high purity Cu,[118]. 5

2 Arrangement of dislocation in a well annealed crystal, [119]. 5

3 Subgrain tilt boundary formed by edge dislocations [120] 7

4 Geometry of node formation in FCC materials of low SFE. Shaded areas are stacking fault, [25]. 7

5 The approximate stacking fault energies of copper and silver alloys and its relationship with dislocation distribution, [26]. 10

6 The difference between slip and twinning, [121]. 10

7 A twinning transformation, [121]. 12

8 Twin stress versus SFE for Cu base alloys, [29]. 12

9 Slip in FCC crystals, [122]. 16

10 Twinning dislocation arrangement at twin-matrix interface, [106]. 16

11 Decreasing solubility of α and β with decreasing temperature. 17

12 Types of interfaces between two crystal structures, [40]. 19

13 a) Hypothetical binary equilibrium diagram, and b) free energy composition curves of elements A and B for temperature T_1, [40]. 22

14 Activation energies of formations $\Delta F_{\beta''}$/ $\Delta F_{\beta'}$/ ΔF_{β} of metastable precipitates β'' and β' and equilibrium precipitate β respectively, [40]. 24

NO PAGE

15 The free energy of formation of spherical embryos as a function of radius for a series of temperatures, [123]. 27

16 Realignment of edge dislocations during polygonization, [124]. 33

17 Recrystallization kinetics for Al deformed 50% and annealed at 350° C, [64]. 33

18 Effect of prior cold work on recrystallized grain size of alpha-brass, [125]. 33

19 Nucleation by subgrain growth. Subgrain boundaries thickly populated by dislocations (dots) have a high misorientation angle, and are most likely to migrate, [66]. 36

20 Schematic representation for the formation of a recrystallized grain by the coalescence of subgrains, [67]. 36

21 Model for strain-induced boundary migration, [66]. 38

22 Potential barrier involved in moving an atom across a grain boundary, [126]. 38

23 Schematic diagram showing the possibilities for interaction between recrystallization and precipitation processes, [76]. 41

24 (a) Discontinuous recrystallization
(b) Discontinuous precipitation
(c) Combined discontinuous reaction
(d) Dispersed particles exerting a retarding force, P_r, [127]. 42

25 Driving force of discontinuous recrystallization versus time for the various temperature ranges of Fig. 23. 45

26 Schematic sketch of continuous recrystallization, [76]. 50

27 Temperature dependence of incubation periods for precipitation (t_p) and recrystallization (t_R) as a function of dislocation density, [76]. 52

NO		PAGE
28	The force acting at the reaction front as a function of dislocation density, [76].	53
29	Vicker's Pyramid Hardness (VPH) versus aging time at 800^{o}C for various degrees of prior deformation.	58
30	As solution treated tensile strength versus aging time at 800^{o}C.	60
31	Cold rolled 5% tensile strength versus aging time at 800^{o}C.	61
32	Cold rolled 30% tensile strength versus aging time at 800^{o}C.	62
33	Cold rolled 60% tensile strength versus aging time at 800^{o}C.	63
34	Grain size versus prior deformation and time of anneal.	65
35	Microstructure of as solution treated at 1200^{o}C. (312x)	66
36	Microstructure of as solution treated + 50 hr. at 800^{o}C. (420x)	66
37	Microstructure of 5% cold rolled (CR) + 10 hr. at 800^{o}C. (150x)	68
38	Microstructure of 5% CR + 50 hr. at 800^{o}C. (352x)	68
39	Microstructure of as 30% CR. (1720x)	69
40	Microstructure of 30% CR + 10 hr. at 800^{o}C. (1330x)	69
41	Microstructure of 30% CR + 50 hr. at 800^{o}C. (1560x)	70
42	Microstructure of 30% CR + 100 hr. at 800^{o}C. (1560x)	70
43	Microstructure of as 60% CR. (420x)	71
44	Microstructure of 60% CR + 10 hr. at 800^{o}C. (470x)	71
45	Microstructure of 60% CR + 51 hr. at 800^{o}C. (625x)	72
46	Microstructure of 60% CR + 51 hr. at 800^{o}C. (2340x)	72
47	Microstructure of 60% CR + 119 hr. at 800^{o}C. (266x)	73
48	Microstructure of 60% CR + 119 hr. at 800^{o}C. (2340x)	73

NO PAGE

49 Carbon Extraction replica of 5% CR + 54 hr. at 800^{O}C. (9,020x) 76

50 Carbon Extraction replica of 60% CR + 10 hr. at 800^{O}C. (12,220x) 76

51 Carbon Extraction replica of 60% CR + 10 hr. at 800^{O}C. (47,520x) 77

52 Carbon Extraction replica of 60% CR + 100 hr. at 800^{O}C. (10,720x) 77

53 Carbon Extraction replica of 60% CR + 100 hr. at 800^{O}C. (10,720x) 79

54 Brightfield of as solution treated condition, showing twin bands. (25,430x) 79

55 SADP of band region in Fig. 54. 80

56 Darkfield of Fig. 54. (30,371x) 80

57 Brightfield of 60% CR condition showing dislocation tanglement. (67,620x) 81

58 Brightfield of 5% CR condition showing twin bands. (30,370x) 81

59 Darkfield of Fig. 58. (30,370x) 82

60 Brightfield of as 30% CR condition showing twin bands. (35,510x) 82

61 Darkfield of Fig. 60. (37,510x) 83

62 Brightfield of as 60% CR condition showing stepped twin bands. (30,370x) 83

63 Darkfield of Fig. 62. (30,370x) 84

NO PAGE

64 Brightfield of 5% CR + 50 hr. at 800°C showing Ni_3Nb precipitate. (19,070x) 84

65 Brightfield of 5% CR + 109 hr. at 800°C showing small NbC particles. (37,510x) 86

66 SADP of long precipitate in Fig. 64 indexed as Ni_3Nb. 86

67 Brightfield of 5% CR + 25 hr. at 800°C showing a deformation twin. (47,520x) 88

68 Brightfield of 30% CR + 10 hr. at 800°C showing Ni_3Nb precipitate. (30,370x) 88

69 Darkfield of Fig. 68. (30,370x) 89

70 Brightfield of 30% CR + 50 hr. at 800°C showing intersecting Ni_3Nb precipitate. (19,010x) 89

71 Brightfield of 30% CR + 50 hr. at 800°C showing intersecting Ni_3Nb precipitate and smaller NbC precipitate. (47,520x) 90

72 Darkfield of 60% CR + 10 min. at 800°C showing small precipitate nucleation. (112,550x) 90

73 Brightfield of 60% CR + 20 min. at 800°C showing intersecting deformation twin bands. 92

74 Darkfield of Fig. 73 showing precipitate formation at twin-matrix intersection. (55,860x) 92

75 Brightfield of 60% CR + 20 min. showing precipitate at interface of adjacent twin bands and matrix. (85,040x) 93

76 SADP of twin area in Fig. 75 showing a loss in coherency between twins with precipitation at interface. 93

77 Brightfield of 60% CR + 20 min. at 800°C showing recrystallized region bordering on cold worked region. (55,860x) 94

78 Brightfield of 60% CR + 100 hr. at 800°C showing spheroidal-shaped Ni_3Nb precipitate. (55,860x) 94

NO PAGE

79 Brightfield of 60% CR + 1 hr. at $800^{\circ}C$ showing nucleation of recrystallized grain in twin band area. (37,510x) 96

80 Brightfield of 60% CR + 2 hr. at $800^{\circ}C$ showing plate-shaped Ni_3Nb in cold worked region of matrix. (37,510x) 96

81 Brightfield of 60% CR + 20 hr. at $800^{\circ}C$. Shows recrystallized twin region with Ni_3Nb precipitate near interfaces. (30,370x) 97

82 SADP of Fig. 81 showing twin orientation of (011) T_1 // (011) T_2 and Ni_3Nb precipitate. 97

83 Darkfield of Fig. 81 showing Ni_3Nb precipitate at interface of twins. (30,370x) 98

84 Brightfield of 60% CR + 2 hr. at $800^{\circ}C$ showing precipitation of recrystallization front and Morié fringe pattern. (67,620x) 98

85 Brightfield of 60% CR + 2 hr. at $800^{\circ}C$ showing various sizes of precipitate in recrystallized region. (25,430x) 100

86 Brightfield of 60% CR + 10 hr. at $850^{\circ}C$ showing plate-shaped precipitate and oblate spheroidal precipitate aligned in rows. (12,670x) 100

87 Brightfield of 60% CR + 10 hr. at $850^{\circ}C$ showing process of agglomeration of oblate spheres. (112,547x) 101

88 Brightfield of 60% CR + 20 hr. at $850^{\circ}C$ showing plate Ni_3Nb and rows of spheroidal precipitate. (10,722x) 101

89 Same as Fig. 88 with magnification of 47,520x. 102

90 Structural diagram for multiphase alloys containing 20% Cr, 10% Mo, 70% Ni and Co, [101]. 105

91 Microstructure of swagged 70% MP35N alloy, [99]. 105

92 Hardness versus % Cold Reduction for MP35N and thesis alloy. 107

93 (a) Free energy versus 1/Temperature schematic for MP35N alloy with 20% cold work. 108

(b) Free energy versus 1/Temperature schematic for thesis alloy with 20% cold work. 108

NO PAGE

94 (a) Free energy versus room temperature deformation for MP35N alloy. 109

(b) Free energy versus room temperature deformation for thesis alloy. 109

95 Binary equilibrium diagram for Co-Nb, [128]. 111

96 Binary equilibrium diagram for Co-Ni, [129]. 111

97 Binary equilibrium diagram for Co-Cr, [129]. 111

98 Binary equilibrium diagram for Cr-Ni, [128]. 112

99 Binary equilibrium diagram for Co-Mo, [128]. 112

100 Free energy versus radius of precipitate. 115

101 Darkfield of fault area in as 5% CR condition. (35,400x) 125

102 SADP of fault region and matrix of Fig. 101 (114) matrix // (110) twin. 125

103 SADP of fault region observed in as 60% CR condition. Pattern matches FCC (112). 126

104 SADP from same area as Fig. 103 only with 23° tilt. Matrix indexed as (210) FCC. 126

105 SADP of same area as Fig. 103 only with 38° tilt. Pattern of matrix fits (321) FCC. 127

106 (a) Schematic representation of diffraction intensity distribution by a thin crystal plate or disc. 129

(b) Schematic relationship of (a) and a rotation of the film plane. 129

107 Schematic relationship between twin plane, film plane, and a diffraction spike. 131

108 Schematic rotation of the film plane about tilt axis. 133

109 SADP of fault area seen in Fig. 101. Same pattern as Fig. 102 only at altered projector lens current. 136

NO PAGE

110 SADP of same area as Fig. 109 only with a relative tilt of 23^{o}. 136

111 Relationship of twin plane normal and initial co-ordinate system of Fig. 109. 138

112 Superposition of Fig. 109 and 110. 138

113 Brightfield of as 60% CR. Fault structure in lower left hand corner. (69,500x) 139

114 SADP of fault structure in Fig. 113. 139

115 SADP of same fault structure in Fig. 113 but at a relative tilt of 18^{o}. Symmetry of SADP is same as that of Fig. 110. 140

116 Relationship of twin plane normal with initial co-ordinate system of Fig. 114. 141

117 Superposition of Fig. 114 and 115. 141

118 SADP of Ni_3Nb precipitate. Shows required indexing of (210) which is forbidden by space group Pmmn but allowed by space group Pma2. 145

119 SADP of Ni_3Nb precipitate. Shows required indexing of (010) which is forbidden by space group Pmmn but allowed by space group Pma2. 145

120 SADP of Ni_3Nb precipitate. Shows required indexing of (120) which is forbidden by space group Pmmn but allowed by space group Pma2. 146

121 SADP of Ni_3Nb precipitate. Indexing fits both space group Pmmn and space group Pma2. 146

CHAPTER 1 INTRODUCTION

Superalloy is the term used to describe an alloy maintaining high strength and corrosion resistance in high temperature application. These alloys have a base element of nickel, chromium, cobalt, iron, or iron-nickel. Since the first patented use of Co-Cr (20-33%) and Co-Cr type alloys by G. Tamman[1] in 1909, Co-base alloys have become increasingly important in superalloy application. The property characteristics that make Co-base alloys attractive include excellent thermal fatigue resistance, high strength above 900°F, relatively high melting point, and good resistance to hot environment of lead and sulphur compounds.[2]

The major alloying constituent of Co-base alloys has been Ni which increases the strength and stabilizes an FCC matrix. Pure Cobalt is allotropic in nature, existing as an FCC structure at high temperature and close-packed hexagonal at room temperature.[3] The transformation is martensitic with an Ms temperature of 417°C. Alloy addition of 30% Ni stabilizes the FCC structure by lowering the Ms temperature to below room temperature.[4] Corrosion resistance is provided by addition of chromium, usually in amounts of 15-22%.

Much work[5,6,7,8,9,10,11] has been done in the past decade in precipitation strengthening these alloys with smaller additions (1-10%) of such elements as Ti, Mo, Al, and Nb. One such alloy developed at the University of Manitoba has the nominal composition of 40% Co, 38% Ni, 17% Co, 5% Nb. The precipitation and aging kinetics of this system on the solution treated condition has already been studied.[5] However, the effect of prior deformation on aging was not considered. It was the intent of this thesis to study these effects on the mechanical properties and microstructure. Such a study is important if thermo-mechanical treatments are considered as a way of improving the properties of this alloy. It includes the three phenomena of plastic deformation, precipitation, recrystallization, and their mutual influence on each other.

The specific approach taken was to study the effects of light (5%), moderate (30%), and heavy (60%) prior deformations on the microstructure and mechanical properties in the pre and post aged conditions. X-ray and electron microscopy techniques were employed to study precipitation and recrystallization behavior, while Vickers pyramid hardness and tensile testing was used to study changes in mechanical properties.

CHAPTER 2 LITERATURE SURVEY

2.1 PLASTIC DEFORMATION

2.1.1 Dislocations and Mechanical Properties

Plastic deformation of a metal at a temperature which is low relative to its melting point (< 0.5 Tm) is called cold working. The energy expended during deformation mostly appears as heat, but a small fraction is stored in the metal in the form of lattice defects (Fig. 1). These are point defects such as vacancies and interstitial atoms, and line defects called dislocations. The majority of the strain energy is stored in the latter. Dislocation densities are expressed in total length of dislocation line per unit volume of material. The density increases progressively with cold work from an initial well annealed value of $10^6 cm^{-2}$ to $10^{11} - 10^{13} cm^{-2}$ with plastic strains of 100%.

It has long been established[12,13] that increasing dislocation density is accompanied by an increasing strength and hardness of the metal and a decreasing ductility. These property changes are due to work-hardening mechanisms involving dislocation generation, multiplication, and mutual interaction.

High strength materials can also be produced theoretically, by reducing the dislocation density to zero, in which case all materials would have the theoretical strength $\approx G/30$.[14] However this is only virtually obtainable in nearly perfect single crystals called whiskers.[15] In real materials, unavoidable dislocations are introduced during solidification, during thermal contraction on cooling, and as a result of phase transformation.

Dislocations are actually fortunate, for they provide the property of ductility needed for the fabrication processes of engineering materials.

2.1.2 Dislocation Arrangement in the Annealed State

In the annealed state, metal crystals typically have a dislocation density of about $10^6 cm^{-2}$. The arrangement of these dislocations has been revealed to be of two basic types: a) three dimensional networks called the Frank nets[16] (Fig. 2); b) planar dislocation networks called tilt and twist boundaries[17,18] (Fig. 3). From elementary dislocation theory, it is known that a dislocation cannot end in a crystal. It must end at the surface of the crystal, form a closed loop, or branch into other dislocations. The latter possibility leads to the formation of nodes, which are points where three or more dislocations meet on the condition that the sum of their Burgers vectors is zero. Such dislocations networks form Frank nets which are believed to have high thermal stability.

The formation of planar dislocation networks arises out of the presence of an excess of dislocations of one sign. Edge dislocations give rise to formation of pure tilt boundaries, and screw dislocations form twist boundaries. Both climb and cross slip are necessary for dislocations to arrange themselves in such configurations which are called low angle boundaries. Regions of the crystal separated by such boundaries differ in orientation by less than 5°.

The driving force for the formation of low angle boundaries is the reduction of strain energy. Long range internal stresses of the dislocations are eliminated by their mutual interaction. However, short range stress fields always remain.

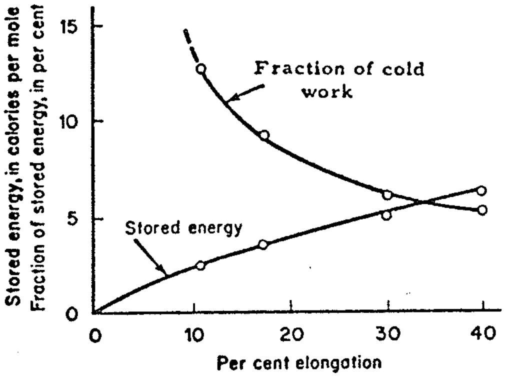

Fig. 1 Stored energy and fraction to total deformation energy stored with elongation of high purity copper, [118].

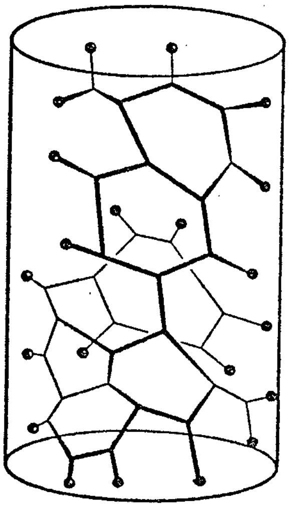

Fig. 2 Arrangement of dislocation in a well annealed crystal; the Frank net, [119].

Solute atoms in a solvent metal manifest their effect on dislocation arrangements through the stacking fault energy of the metal. The addition of solute atoms can lower the stacking fault energy (SFE), resulting in a tendency for a dislocation to dissociate into partial dislocations with a faulted region in between. The strain energy of a dislocation is proportional to b^2 through the general strain energy relation of:

$$E = \alpha G b^2$$

where $\alpha \simeq 0.5 - 1.0$, and G is the shear modulas. According to Frank's rule, if b_1, b_2, and b_3 are permissible Burgers vectors in a particular crystal lattice, a dislocation with the Burgers vectors b_3 will split up into the dislocation b_1 and b_2 if $b_3^2 < b_1^2 + b_2^2$. In FCC metals and alloys, such dissociations can take place on the slip plane {111} and the resultant reaction is described as:

$$a/2\ [110] \rightarrow a/6\ [211] + a/6\ [12\bar{1}]$$

where 'a' is the lattice parameter.

The partial dislocations have components of the same sign and will repel each other, forming a ribbon of stacking fault between them, which has a characteristic energy called the stacking fault energy (ergs/cm^2). This energy provides a force tending to pull the dislocation together. Metals of high stacking fault energy will have whole dislocations, while those of relatively low SFE (< 30 ergs/cm^2) tend to have extended dislocations.

The geometry of the Frank net associated with metals of low SFE has been described by Whelan[20] and is shown in Figure 4. The partial dislocations are constricted at nodal junctions while extended along their free length. Partial dislocations by themselves cannot cross slip or climb. They must be constricted to form a whole dislocation of some finite length before these mechanisms of dislocation movement can operate. Therefore,

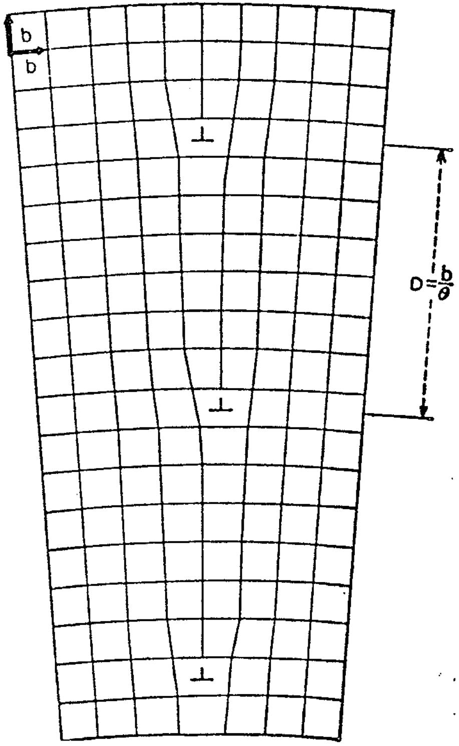
b
b
D=$\frac{b}{\theta}$

Fig. 3 Subgrain tilt boundary formed by edge dislocations, [120].

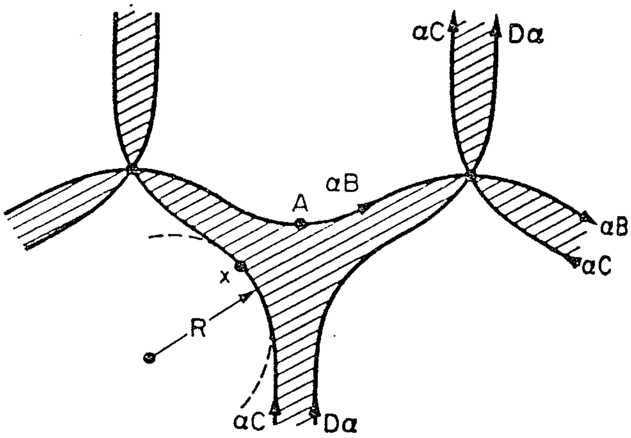
αC
Dα
αB
A
αB
αC
x
R
αC
Dα

Fig. 4 Geometry of node formation in FCC materials of low SFE. Shaded areas are stacking fault, [25].

lowering the stacking fault energy by solute atoms hinders the formation of low angle boundaries. This is an observation made in many alloy systems (Cu-Al)[21,22], (Cu-Zn, Al, Ge, Sn, or Si)[23], (Ag- Zn, or Al and Ni-Co).[24]

2.1.3 Dislocation Arrangement in Polycrystals Deformed at Room Temperature

The plastic deformation of annealed metals and alloys causes an increase in flow stress, and the phenomenon is called strain hardening. It is the result of rapid dislocation multiplication and their interaction with one another and with obstacles, such as precipitates, in the slip planes. The dislocation arrangements are generally similar between materials of different crystal structures, and depend mainly on one material variable, the SFE.[25]

In materials that have SFE > 30 ergs/cm^2, the process of cross slip and climb are relatively easy. Initially, up to strains of approximately 10%, multiplication mechanisms result in formation of tangles of dislocations which eventually link up to form well defined cell structure. The cell interiors are relatively free from dislocations and the cell walls tend to lie along certain crystallographic planes.[26] The cell walls are called tangles because of their jagged, twisted, and irregular array nature. Further deformation increases the density of dislocation and sharpness of the cell wall, resulting in an irregular misorientation between the cells of up to 5°.[27] There is little tendency towards refinement of the cell size with greater deformation. However cold rolling tends to elongate the cells in the direction of rolling, often exhibiting a preferred orientation.

When the SFE is less than 30 ergs/cm^2, the process of extended dislocation changes the appearance of dislocation arrangement. There is little tendency to form cellular structure even at high strains. Cross slip is inhibited, forcing dislocations to remain on their slip planes, resulting in pile ups at obstacles such as grain boundaries. At low strain, the prominent features are bands of extended dislocations (stacking faults) and planar pile up arrays. At high strain there is some tendency to form a very ragged tangled cellular structure.[26] When solute atoms lower the SFE of a metal, the extended dislocation structure is promoted. Different alloys of the same SFE have similar dislocation arrangements, independent of the species of alloying elements. This has been summarized for Cu and Ag alloy by Swann[26] in Figure 5.

2.1.4 Deformation Twinning

2.1.4.1 General Characteristics

Twinning and slip are modes of plastic deformation and both result in a net shear of the lattice. The basic difference in lattice translation between the two is illustrated in Figure 6. In slip, deformation occurs on relatively few discreet lattice planes for a given volume. It has a two dimensional character, and within a volume the majority of atoms remain fixed with respect to each other. In deformation twinning, the total shear is uniformly distributed throughout the volume by a co-operative movement of atoms in which individual atoms move a fraction of the interatomic spacing relative to each other. The resulting lattice of twin volume is a mirror image of the parent lattice across the plane separating the two. This symmetry plane, usually of low indices is called the twinning plane and is illustrated in Figure 7.

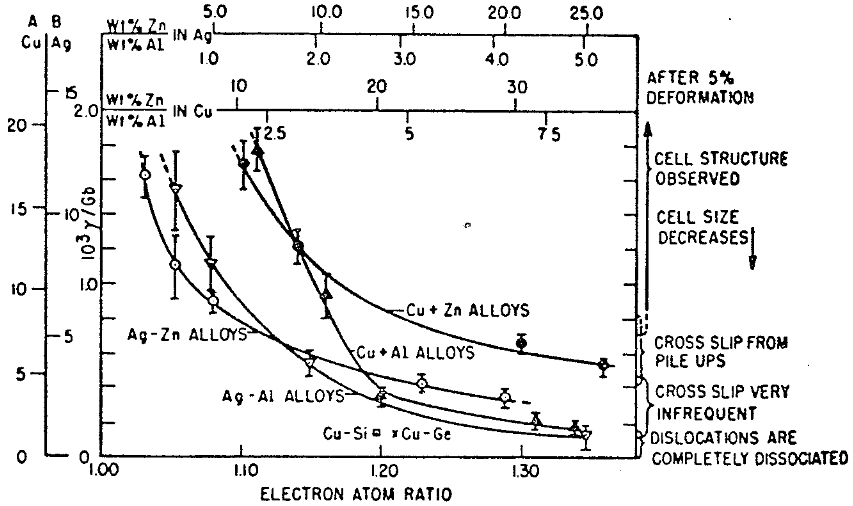

Fig. 5 The approximate stacking fault energies of copper and silver alloys are given by columns A and B. The relationship with dislocation distribution is described in the column on the right, [26].

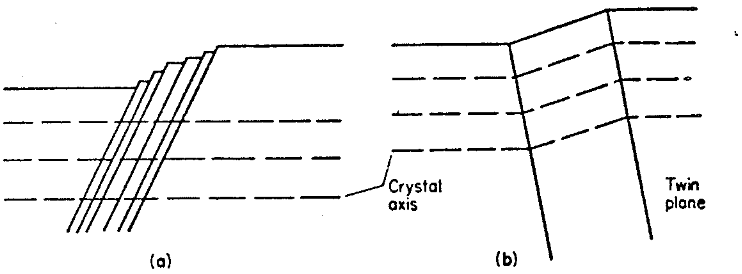

Fig. 6 The difference between (a) slip and (b) twinning, [121].

The process of twinning is frequently a catastrophic event resulting in a sharp load drop and serrated yielding in a tension test. The large energy release can sometimes result in an audible sound such as the "cry" of tin in deformation. Twinning is an important mode of deformation in metals where possible slip systems are limited such as BCC and CPH crystal structures. If a crystal is in an unfavourable orientation for slip, twinning may occur to align the possible slip systems more favourably.

In FCC metals, which have many slip systems, twinning is not considered a dominant mode of deformation. It occurs only under a highly resolved shear stress of a work hardened state, which can be obtained at low temperatures of deformation.[28] It also can be found to occur more readily in metals and alloys which possess a low SFE, in which case slip would be inhibited. Venables[29] has plotted results for Cu alloys which demonstrate a tendency for a lowering of twinning stress with decreasing SFE (Fig. 8). He argues that a transition occurs in twinning between high and low SFE materials, the latter twin profusely on a fine scale without noticable load drop. He contends that twin nucleation is easier for low stacking fault materials, where propagation of twins through forest dislocations is difficult. With high SFE, twin nucleation is the critical step, giving rise to the catastrophic load drop and Lüders band growth in a tension test.

Also in this review[29], Venables concludes that there is little definite orientation or temperature variation of the twin stress in FCC metals. Composition of the alloy is thought to be important because of variation in SFE.

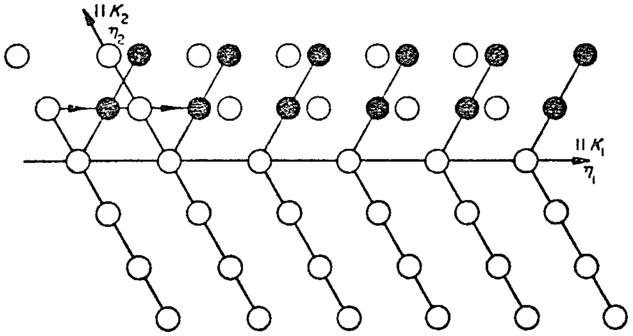
|| K_2
η_2
|| K_1
η_1

Fig. 7 A twinning transformation, [121].

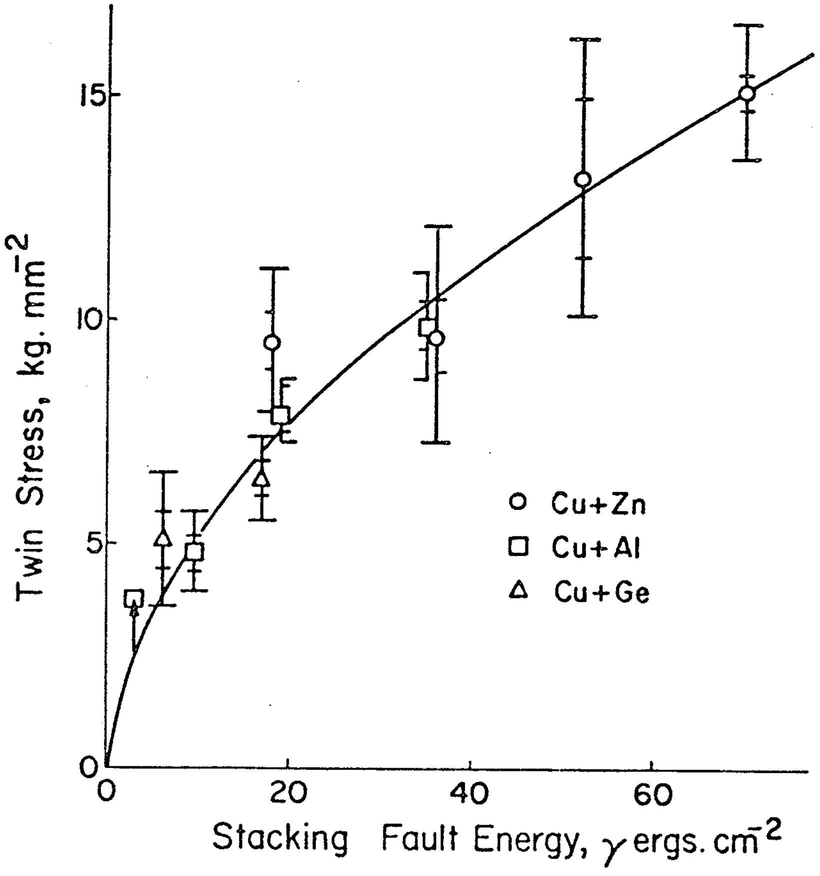

Fig. 8 Twin stress versus stacking fault energy for copper base alloys, [29].

2.1.4.2 Twinning Mechanism for FCC Metals

The characteristic stacking sequence of (111) planes in FCC structure is:

A B C A B C A B C

The atomic arrangement of the atoms in a (111) plane is shown in Figure 9 with the atomic positions of the planes immediately above and below indicated. The stacking sequence of close-packed planes encountering a twin boundary is given by:

A B C A B A C B A

As with slip, deformation twinning takes place at stresses far below the theoretical shear strength for a perfect crystal. It follows that twinning must occur by a continuous growth of the twinned material on an atomic scale and not by the simultaneous movement of all atoms involved. Slip occurs on {111} planes in <110> directions and is the result of numerous whole dislocations passing over few slip planes. The amount of shear dislplacement for one dislocation and shear direction is illustrated by vector b_1 of Figure 9. Twinning, on the other hand, is the result of homogeneous shear and is equivalent to the passage of partial dislocation on successive planes. The shear displacement and direction on each plane is represented by the vector b_1 or b_2 in Figure 9. Dislocation models to account for this shear in deformation twinning can do so in one of two ways.[30] These are the initiation of identical partial dislocationsin every lattice plane, as described by the homogeneous twin nucleation model, or the passage of a simple partial dislocation moving from one plane to the next, as described by the pole mechanism.

The homogeneous nucleation of stable twin nuclei, although no application of it to FCC metals could be found, is outlined here for the sake of completeness. It was first considered by Orowan,[31] who concluded that twin nuclei would arise at stress concentrators which could increase the locally applied stress to the theoretical twinning stress. Studies on Zinc[32] concluded that the piling up of slip dislocations against a suitable obstacle was a sufficient stress concentrator. Acceptance of this model requires that one accepts the creation of partial dislocations out of a perfect lattice. A stable nucleus could propagate by their motion, but increasing thickness of the twin would require repetitive nucleation of twinning dislocations at the twin-matrix interface. Experimental verification of this model has been found in several studies.[33,34,35]

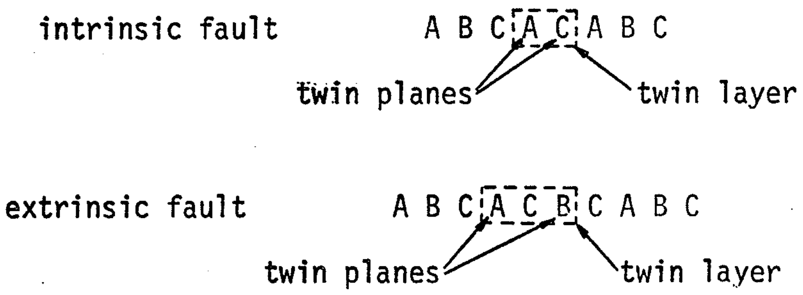The pole mechanism of deformation twinning can be applied to any crystal structure and carries with it the concepts of SFE, partial dislocation, and dislocation interaction. For FCC structures, stacking fault areas are bounded by Shockley a/6 <211> type partials. These areas can be regarded as a layer of twinned material, which, depending on the nature of the fault, has the following sequence: